Inorganic Chemistry

Article

pubs.acs.org/IC

Comparison of the Site Occupancies Determined by Combined Rietveld Refinement and Density Functional Theory Calculations: Example of the Ternary Mo−Ni−Re σ Phase

Khurram Yaqoob, Jean-Claude Crivello, and Jean-Marc Joubert*

Chimie Métallurgique des Terres Rares, Institut de Chimie et des Matériaux Paris-Est, CNRS, Université Paris-Est Créteil, 2−8 rue Henri Dunant, 94320 Thiais Cedex, France

Supporting Information

ABSTRACT: The site occupancies of the Mo−Ni−Re σ phase have been studied as a function of the composition in the ternary homogeneity domain by both experimental measurements and calculations. Because of the possible simultaneous occupancy of three elements on the five sites of the crystal structure, the experimental determination of the site occupancies was achieved by using combined Rietveld refinement of X-ray and neutron diffraction data, whereas calculation of the site occupancies was carried out by using the density functional theory results of every ordered (i.e., 3^5 = 243) configuration appearing in the ternary system. A comparison of the experimental and calculation results showed good agreement, which suggests that the topologically close-packed phases, such as the σ phase, could be described by the Bragg−Williams approximation (i.e., ignoring the short-range-order contributions). On the other hand, the atomic distribution on different crystallographic sites of the Mo−Ni−Re σ phase was found to be governed by the atomic sizes. Ni, having the smallest atomic size, showed a preference for low-coordination-number (CN) sites, whereas Mo, being the largest in atomic size, preferred occupying high-CN sites. However, the preference of Re, having intermediate atomic size, varied depending on the composition, and a clear reversal in the preference of Re as a function of the composition was evidenced in both the calculated and experimental site-occupancy results.

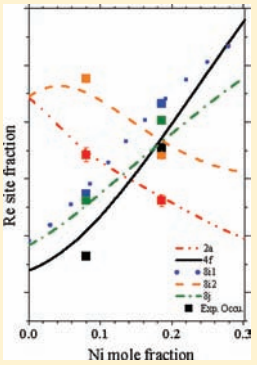

INTRODUCTION

The determination of site-occupancy data for binary compounds by Rietveld refinement is a rather well-established procedure. However, obtaining the same types of data for sites in which three elements may be present simultaneously is a more challenging task. To solve this problem, one should use combined Rietveld refinement of different types of diffraction data in which the scattering contrast between the elements is different, for example, X-ray (XRD) and neutron diffraction (ND) data when the relative scattering in the two techniques is also adequate. On the other hand, density functional theory (DFT) calculations combined in the frame of the Bragg−Williams (BW) approximation may yield calculated site occupancies but are sometimes limited by the large number of configurations one has to calculate (3^s in the case of a ternary phase with s sites).

The crystal structure of the σ phase (structure type FeCr, space group $P4_2/mnm$, 30 atoms per unit cell, five inequivalent sites: 2*a*, 4*f*, $8i_1$, $8i_2$, 8*j*) is shown in Figure 1. It is a hard brittle intermetallic compound and has a deleterious effect on the mechanical properties of many technologically important systems. The main features of the σ phase include non-stoichiometry, which is accommodated by substitution on different sites of its crystal structure, and its ability to accept wide homogeneity ranges. Qualitatively, as usual for the Frank−Kasper phases, larger atoms show a preference for the sites with high coordination number (CN = 15 and 14), whereas smaller atoms occupy the sites with low coordination number (CN = 12).[1] However, determination of the actual exact site occupancies is important for thermodynamic modeling of the σ phase. Several investigations have been made for the quantitative determination of site occupancies in binary systems that have been summarized previously.[1] However, the work for determination of the site occupancies in ternary systems has recently been started and at present, according to our knowledge, it has been the subject of only one experimental[2] and two theoretical investigations.[3,4]

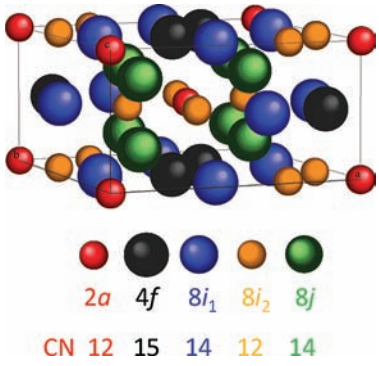

Figure 1. Crystal structure of the σ phase.

Received: November 21, 2011
Published: February 22, 2012

 © 2012 American Chemical Society dx.doi.org/10.1021/ic202479y | *Inorg. Chem.* 2012, 51, 3071−3078

The study of the ternary σ phase is also of primary importance because it may offer the possibility studying a dual preference for the intermediate size atom depending on the composition proportion of the other two elements. This behavior was recently reported for Re in the Cr−Mo−Re σ phase.[3] One of the motivations for selecting the Mo−Ni−Re σ phase for the present study was to verify the dual preference of the intermediate size atom in the studied system. In addition, the large extension of the binary Mo−Re σ phase into the ternary region[5] permitting the study of the variation of the site occupancies as a function of the composition and the importance of the Mo−Ni−Re system for the development of Ni-based superalloys made it an interesting choice for the study of the ternary σ phase.

During the present investigation, a complete structural characterization of the ternary σ phase with particular emphasis on determination of the site occupancies as a function of the composition has been carried out. Unlike previous studies,[2−4] the site occupancies were determined by both experimental and theoretical methods. The reason for using two different approaches is to be able to compare their results and to check their validity. The experimental determination of site occupancies was accomplished by combined Rietveld analysis of XRD and ND data, whereas the theoretical approach for site-occupancy determination was based on the estimation of heats of formation by first-principles calculations. Finite temperature properties, such as site occupancies, were determined using the BW approximation, which ignores the short-range order within the defined sublattices. In spite of this simplification, the latter already gave excellent agreement with experimental studies on the σ phase of binary systems.[6−8] However, a comparison of the site occupancies determined experimentally with DFT predictions for the ternary σ phase has never been done before and is the subject of the present study.

EXPERIMENTAL DETAILS

Sample Preparation and Annealing. The materials used for the preparation of the ternary alloys consisted of pure metal powders (Mo, Sigma Aldrich, <150 μm, 99.99%; Ni, Alfa Aesar, <125 μm, 99.996%; Re, Alfa Aesar, <44 μm, 99.99%). These powders were mixed in an agate mortar, compacted into pellets of different compositions, and subjected to arc melting under an argon atmosphere. The alloys were remelted five times and rotated upside down between each melting to achieve better homogenization. For the sake of reaching equilibrium, the alloys were annealed at 1873 K for 9 h. An annealing treatment of the samples was performed in a high-frequency induction furnace in a water-cooled copper crucible under an argon atmosphere, and the sample temperature was measured with the help of an optical pyrometer. After annealing, the samples were quenched by turning off the induction heating and rapid cooling of the sample took place by the water-cooled copper crucible.

Chemical Characterization. Prior to the structural characterization, part of each sample was polished and investigated with the help of electron probe microanalysis (EPMA; CAMECA SX100) using pure elements as standards. Large numbers of data points were measured to determine the phase composition and homogeneity. The phase composition was averaged from the point measurements performed on that phase, and the calculated standard deviation of these measurements represented the phase homogeneity.

Structural Characterization. For structural characterization, XRD and ND measurements were performed by using a conventional powder method. All samples, by virtue of their high brittleness, were easily reduced to a fine powder (<63 μm).

Powder XRD measurements were performed at room temperature with Cu Kα radiation on a Bruker D8 Advance diffractometer (Bragg−Brentano geometry) equipped with a rear graphite monochromator. The X-ray data collection conditions include $5° \leq 2\theta \leq 120°$, a step size of 0.04°, and a total counting time of 63 h to obtain high data statistics.

ND measurements were performed at Laboratoire Léon Brillouin (LLB; common laboratory CEA-CNRS), Saclay, France, using a 3T2 instrument. The sample in powder form (7.5 g, <63 μm) was introduced into a sample holder consisting of a vanadium cylinder (diameter 6 mm) supported on a cadmium-protected aluminum cylinder. The measurement was performed at room temperature with the Debye−Scherrer geometry in the presence of five detectors. For each pattern, data were recorded in the angular range $5° \leq 2\theta \leq 121°$ with a step size of 0.05° by using neutrons of wavelength 1.2253 Å.

To determine site occupancies, the combined Rietveld analysis of XRD and ND data was conducted using the *FULLPROF*[9] program in the multipattern mode. For refinement of the X-ray data, the background was interpolated between the peaks, whereas for the neutron data refinement, a polynomial background was used. The pseudo-Voigt function was used to define the peak shape in both XRD and ND patterns. Because Re presents the nonnegligible absorption coefficient for neutrons, an absorption correction was also applied by calculating the values of the absorption coefficient (μ_r) for each composition. To calculate the absorption coefficient, the density of noncompacted powders was estimated to be 40% of the density of the material. The values of absorption coefficients (μ_r) calculated for each composition are presented in Table 1.

COMPUTATIONAL DETAILS AND METHODOLOGY

The first-principles calculations were performed by using DFT, as implemented in the Vienna ab initio simulation package.[10,11] Previous calculations on binary Mo−Re[8] and Ni−Re σ phases[12] were done with the PW91 exchange−correlation energy functional,[13] but for the present work, every ordered Mo−Ni−Re σ ternary configuration i.e., $3^5 = 243$ configurations, was calculated with the PBE functional.[14] An energy cutoff of 400 eV was used for the plane-wave basis

Table 1. Rietveld Refinement Details of Experimentally Studied Compositions

	N_1	N_2	N_3
nominal composition	$Mo_{0.486}Ni_{0.08}Re_{0.426}$	$Mo_{0.259}Ni_{0.201}Re_{0.540}$	$Mo_{0.533}Ni_{0.201}Re_{0.266}$
EPMA composition	$Mo_{0.49(2)}Ni_{0.08(1)}Re_{0.43(2)}$	$Mo_{0.256(2)}Ni_{0.186(6)}Re_{0.558(6)}$	$Mo_{0.52(1)}Ni_{0.19(1)}Re_{0.29(2)}$
space group	$P4_2/mnm$	$P4_2/mnm$	$P4_2/mnm$
a (Å)	9.5262(2)	9.3392(2)	9.4018(4)
c (Å)	4.9605(1)	4.9072(1)	4.9134(2)
μ_r(ND)	0.2925	0.3825	0.2404
R_B(XRD), R_B(ND)	7.19, 3.32	4.95, 3.41	4.50, 2.76
profile parameters	4 for each pattern	4 for each pattern	4 for each pattern
intensity parameters	17	17	17

dx.doi.org/10.1021/ic202479y | *Inorg. Chem.* 2012, 51, 3071−3078

set, and a dense grid of k points in the irreducible wedge of the Brillouin zone ($8 \times 8 \times 15$ k-points meshing) was used with the sampling generated by the Monkhorst–Pack procedure.[15] For each of the 243 ordered configurations, successive relaxations (internal atomic coordinates and the lattice parameters, i.e., a and c) were done to fully relax the tetragonal cell structure. The final calculation was performed using the tetrahedron method with Blöchl corrections.[16] The self-consistent total energy calculations converged to less than 0.1 meV. From calculation of the pure elements in their stable element reference (SER) state, the heat of formation $\Delta H^{\text{for},\sigma}_{ijklm}$ at 0 K of every (i, j, k, l, m = Mo, Ni, Re) σ configuration was obtained by the total energy differences written below. The fcc-Ni has been calculated in spin-polarized states.

$$\Delta H^{\text{for},\sigma}_{ijklm} = E^{\sigma}_{ijklm} - c_{\text{Mo}}E^{\text{bcc}}_{\text{Mo}} - c_{\text{Ni}}E^{\text{fcc,mag}}_{\text{Ni}} - c_{\text{Re}}E^{\text{hcp}}_{\text{Re}}$$

c_{Mo}, c_{Ni}, and c_{Re} are the mole fractions of the Mo, Ni, and Re elements, respectively.

On the basis of the compound energy formalism,[17−19] the five-sublattice model $(i)_2(j)_4(k)_8(l)_8(m)_8$ is used, in conformity with the site multiplicities of the σ-crystal structure. The Gibbs energy $G^{\sigma,\text{BW}}(\{x_i\},T)$ is defined at a finite temperature T by using the BW approximation, i.e., considering only the configurational entropy and neglecting the entropy from atomic correlations and excess interaction parameters within the sublattices:

$$G^{\sigma,\text{BW}}(\{x_i\}, T) = \sum_{i,j,k,l,m=\text{Mo,Ni,Re}} [y_i^{(2a)} y_j^{(4f)} y_k^{(8_{i_1})} y_l^{(8_{i_2})} y_m^{(8_j)}] \times \Delta H^{\text{for},\sigma}_{ijklm} + RT \sum_s a^{(s)} \sum_{i=\text{Mo,Ni,Re}} y_i^{(s)} \ln(y_i^{(s)})$$

R is the gas constant, $a^{(s)}$ the multiplicity, and $y_i^{(s)}$ the site fraction of element i on site s.

More details about the methodology can be found in previous papers.[3,8]

EXPERIMENTAL RESULTS

The homogeneity domain of the σ phase in the 1873 K isothermal section of the Mo–Ni–Re system extends from the binary Mo–Re system, in which the homogeneity domain is 52 ± 2–70 ± 2 atom % Re,[20] deeply into the ternary region. The exact location of the homogeneity domain of the Mo–Ni–Re σ phase will be published with complete determination of the phase diagram[5] but is shown only as indicative in Figure 2. To study the atomic distribution of the constituent elements, i.e., Mo, Ni, and Re, at the different crystallographic sites as a function of the composition, three compositions (named as N_1, N_2, and N_3) situated at the borders of the homogeneity domain of the σ phase and along the two lines Mo_2Re–Re_2Ni and $MoRe_2$–Mo_2Ni were prepared and characterized. As expected, EPMA and conventional powder XRD results confirmed the single-phase character of each sample. The small difference between the measured and nominal compositions reported in Table 1 was attributed to the evaporation of Ni during melting

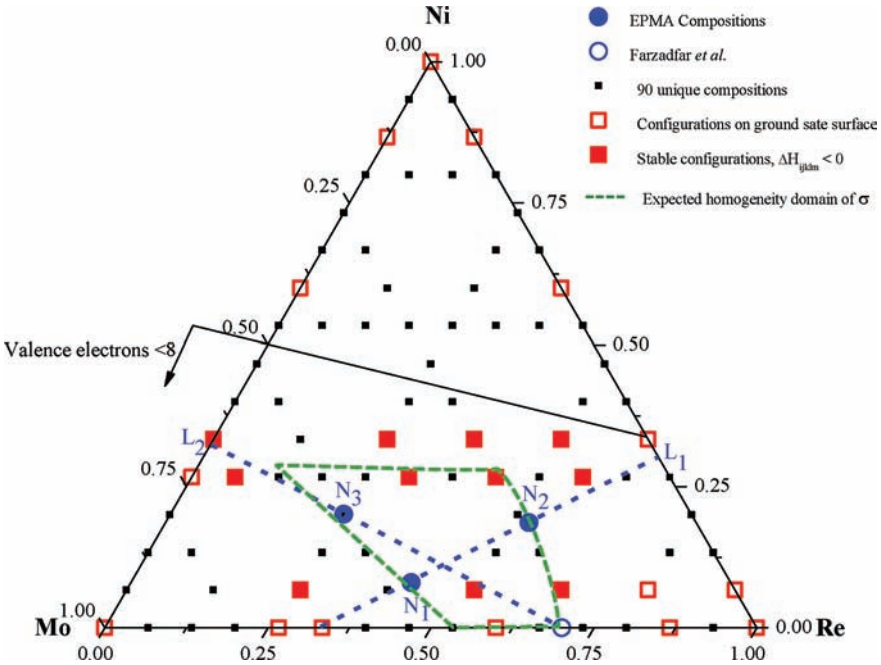

Figure 2. Plot of the compositions studied experimentally and by DFT calculations. The area surrounded by green dashed lines represents the indicative homogeneity domain of the Mo–Ni–Re σ phase at 1873 K. The positions of the experimentally studied compositions, named as N_1, N_2, and N_3, are symbolized by blue filled circles, whereas the empty blue circle represents the composition studied previously.[21] The two blue dashed lines, i.e., L_1 and L_2, correspond to sections studied by DFT calculations. The 90 unique compositions generated during DFT calculations by the ordered distribution of three elements on the five sites of the σ phase are indicated by black squares. Among the 90 unique compositions, 26 compositions are located on the ground-state surface and are symbolized by red squares, whereas among 26 compositions, 11 compositions present negative heats of formation and are indicated by red filled squares.

dx.doi.org/10.1021/ic202479y | Inorg. Chem. 2012, 51, 3071–3078

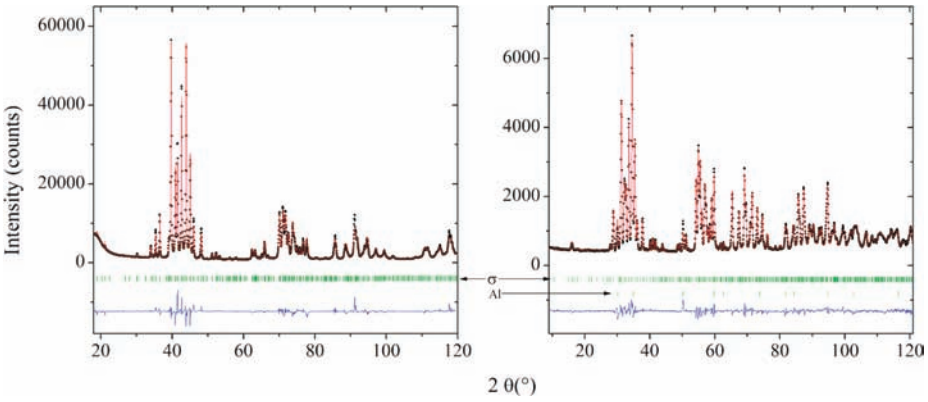

Figure 3. Combined Rietveld refinement of the XRD (left) and ND (right) patterns of the sample composition N_2. The experimental curves are symbolized as black dots, calculated ones as red lines, Bragg positions as vertical green marks, and the difference between the experimental and calculated curves is symbolized as a blue line situated under the vertical green marks.

because of its high vapor pressure at the extremely high melting temperatures of the alloys (the binary Mo−Re σ phase melts at 2918 K[20]). The positions of the measured compositions in the ternary section are represented by blue filled circles in Figure 2. In addition to the prepared compositions, the site-occupancy data of the binary Mo−Re σ phase of composition $Mo_{0.299}Re_{0.701}$, represented by the empty blue circle in Figure 2, were taken from the literature.[21]

The separate XRD refinement of the studied compositions yielded strongly negative values of displacement parameters (B), indicating the presence of microabsorption phenomena in XRD measurements, because both are strongly correlated. Refinement of displacement parameters along with the microabsorption correction using one pattern refinement was not possible. However, during the combined refinement of the XRD and ND patterns, in which the value of B was also constrained by the ND pattern, microabsorption correction was applied. As a result, reasonable values of the displacement parameters were obtained. For the studied compositions, the site fractions of constituent elements at the five crystallographic sites of the σ phase were determined by combined Rietveld refinement of XRD and ND data. During the refinement, each pattern was assigned equal weights. The distribution of the elements was constrained in such a way that it reproduces the measured composition and full occupancy of all atom sites. As a result, there were two unknown occupancy factors per site on four sites, i.e., eight variables. The occupancy of the elements on the fifth site was constrained by the occupancies on the other four sites. The method for introducing such constraints in Rietveld refinement programs has been previously described.[22−24] For each composition, a total of 17 intensity parameters, including 7 coordinates, 2 displacement parameters (one for the sites with CN = 12 and the other for the higher CN sites), and 8 occupancy factors, were refined. The values of R_B considered as a measure of the quality of fit, along with other refinement details, are given in Table 1.

As an example, the diffraction patterns in the form of Rietveld plots of the sample composition N_2 are presented in Figure 3.

The Rietveld analysis of all ND patterns disclosed the presence of several peaks not present in any of the XRD patterns. Investigation of these additional peaks revealed that these peaks correspond to the aluminum cylinder intercepting the neutron beam accidently. Normally, the aluminum cylinder supporting the vanadium sample holder is very well protected by cadmium, which does not appear to be the case in the present measurements, and as a result, we find peaks corresponding to aluminum in the ND patterns. These additional peaks were also taken into account during refinement of the ND patterns.

For the studied compositions, occupancy factors of the constituent elements at each site of the Mo−Ni−Re σ phase are presented in Table 2. The negative occupancy factors were obtained at some sites that for comparison purposes were not constrained to be positive.

Table 2. Occupancy Factors for the Compositions N_1, N_2, and N_3

			occupancy (atom)		
site	CN	element	N_1 ($Mo_{0.49(2)}$ $Ni_{0.08(1)}$ $Re_{0.43(2)}$)	N_2 ($Mo_{0.256(2)}$ $Ni_{0.186(6)}Re_{0.558(6)}$)	N_3 ($Mo_{0.52(1)}$ $Ni_{0.19(1)}Re_{0.29(2)}$)
2*a*	12	Mo	0.18(9)	−0.15(10)	0.07(9)
		Ni	0.85	1.50	1.29
		Re	0.97(5)	0.65(4)	0.64(4)
4*f*	15	Mo	3.63(12)	1.82(13)	3.49 (12)
		Ni	−0.14	0.15	−0.12
		Re	0.51(6)	2.03(6)	0.63(6)
$8i_1$	14	Mo	4.88(20)	2.86(19)	5.41(19)
		Ni	0.33	−0.19	0.08
		Re	2.79(10)	5.33(9)	2.51(8)
$8i_2$	12	Mo	0.36(17)	0.04(17)	0.75(15)
		Ni	1.62	4.09	4.33
		Re	6.02(9)	3.87(9)	2.92(8)
8*j*	14	Mo	5.65	3.12	5.87
		Ni	−0.25	0.03	0.13
		Re	2.60	4.85	2.00

DFT Calculation Results. First of all, the results on the three binary systems are presented. In comparison with calculations of the Mo−Re[8] and Ni−Re[12] systems made with the PW91 functional, results obtained in PBE present very similar $\Delta H^{for,\sigma}_{ijklm}$. Differences are less than 1 kJ/mol of atoms and lead to insignificant modifications on the finite temperature properties, such as the site occupancies (found to be similar in both Mo−Re and Ni−Re systems). A more careful analysis on the relaxed crystal parameters shows that calculations with PBE are in slightly better agreement with the experimental results and confirms the choice of using this functional for the present

dx.doi.org/10.1021/ic202479y | Inorg. Chem. 2012, 51, 3071−3078

Table 3. Energetic and Crystallographic Property Comparison between Experiments and Calculations with Two Different Functionals in the Mo_xRe_{1-x} System

	$x \sim 0.33$			$x \sim 0.4$			
	ΔH (kJ/mol)	V (Å^3)	c/a	ΔH (kJ/mol)	V (Å^3)	c/a	ref
Exp		455.35	0.520		457.81	0.519	21
PW91	+5.29	460.76	0.513	+1.07	463.05	0.511	8
PBE	+5.42	459.41	0.513	+1.14	461.67	0.511	present work

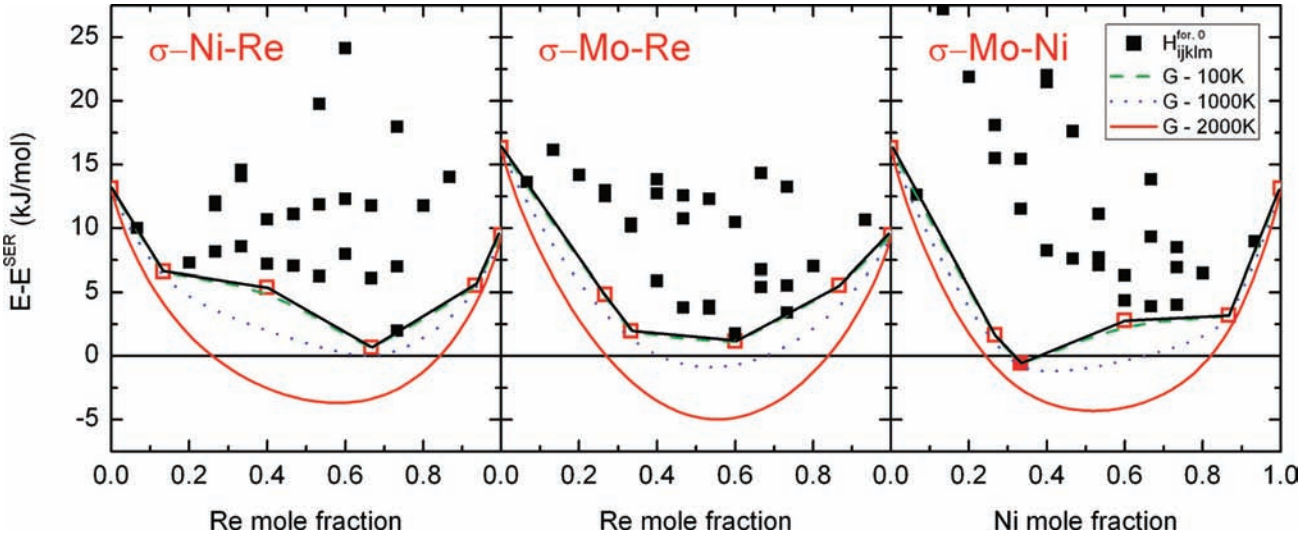

Figure 4. Calculated heats of formation $\Delta H^{for,\sigma}_{ijklm}$ of the 32 configurations in the three binary Ni–Re, Mo–Re, and Mo–Ni σ phases with respect to SER states. The Gibbs energy lines obtained in the BW approximation are displayed at 100, 1000 and 2000 K.

work. As an example, a comparison is made for two compositions in the Mo–Re system and is given in Table 3.

The heat of formation calculation of the $2^5 = 32$ configurations and the $G^{\sigma,BW}(\{x_i\},T)$ curves computed at $T = 100$, 1000, and 2000 K for the three binary systems are displayed in Figure 4.

As expected, the scatter of $\Delta H^{for,\sigma}_{ijklm}$ points is more important in the Mo–Ni system because of the larger atomic radii difference between the Mo and Ni atoms, in comparison with Re–Ni and Mo–Re. All binary $\Delta H^{for,\sigma}_{ijklm}$ are positive, except the (i,j,k,l,m) = NiMoMoNiMo configuration. The latter corresponds to the ideal Mo_2Ni composition with occupation of the low CN sites by Ni and high CN sites by Mo. For each system, the ground-state line is drawn. It is defined as the line joining the six most stable configurations obtained by a single atom permutation on every five sites. For the Mo–Re system, this line is convex and the following sequence is observed: MoMoMoMoMo → MoMoMoReMo → ReMoMoReMo → ReMoReReMo → ReMoReReRe → ReReReReRe. On the contrary, a change of concavity is observed in both Mo–Ni and Ni–Re systems, yielding a miscibility gap. Only above $T = 1000$ K, every Gibbs energy $G^{\sigma,BW}(\{x_i\},T)$ curve is convex and a single phase is stable in the whole concentration range.

From the $3^5 = 243$ configurations generated in the ternary system, 90 are unique compositions, and among them, 26 configurations are on the ground-state surface. They are represented in Figure 2 by squares. In comparison with Cr–Mo–Re, it is interesting to note that the σ phase is more stable in the Mo–Ni–Re system with 11 negative $\Delta H^{for,\sigma}_{ijklm}$ among the 26 ground-state configurations (versus the nonnegative formation enthalpy configuration and 19 on the ground-state surface for Cr–Mo–Re). These 11 configurations with negative $\Delta H^{for,\sigma}_{ijklm}$ present a Ni composition of less than 33%. The most stable configuration is with NiMoReNiMo ($Mo_{0.40}Ni_{0.33}Re_{0.27}$). Because Mo_2Ni is the only stable binary composition with $\Delta H^{for,\sigma}_{ijklm} < 0$, it is expected that the σ phase, which exists experimentally in the binary Mo–Re system, would extend in the ternary region toward the Mo_2Ni direction. This assumption has been verified experimentally.[5]

In addition, as shown in Figure 2, both the suggested experimental phase field of σ and the calculated stable configurations are situated below the solid black line representing a valence electron concentration of 8. This result is in agreement with the empirical rule stating that the σ phase forms for an average electron concentration range between 5.5 and 8.[1,25]

The $G^{\sigma,BW}(\{x_i\},T)$ surface computed at $T = 100$ K is represented in Figure 5. The change of concavity reveals the presence of miscibility gaps at this low temperature. The corresponding isocontour plot of this surface is also represented for the same temperature $T = 100$ K and also for $T = 1000$ K. At $T = 1000$ K, the $G^{\sigma,BW}(\{x_i\},T)$ surface presents a single minimum, and accurate calculation shows that the miscibility gap disappears at $T = 984$ K.

DISCUSSION

Because the substitutional disorder in the ternary σ phase involves three elements, accurate experimental determination of the site occupancies required at least two diffraction data sets with large scattering contrast among the constituent elements in each data set and different scattering contrast among the elements in two data sets. The ternary system under study is well chosen because it obeys both conditions. The elements constituting the studied system give large scattering contrast in both XRD and ND techniques, as indicated by their atomic

dx.doi.org/10.1021/ic202479y | Inorg. Chem. 2012, 51, 3071–3078

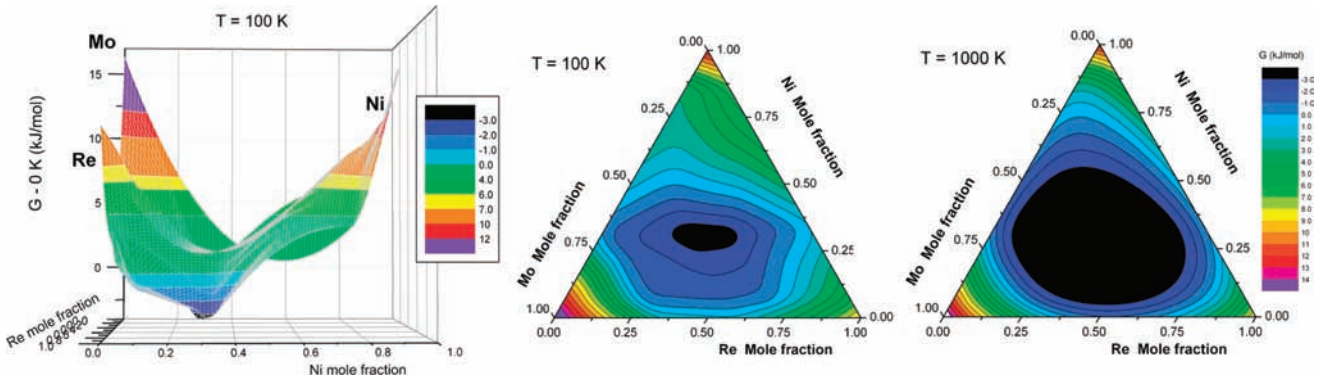

Figure 5. Gibbs energy surface of the Mo−Ni−Re σ phase obtained in the BW approximation displayed at 100 K. Corresponding isocontour plots at 100 and 1000 K are also presented.

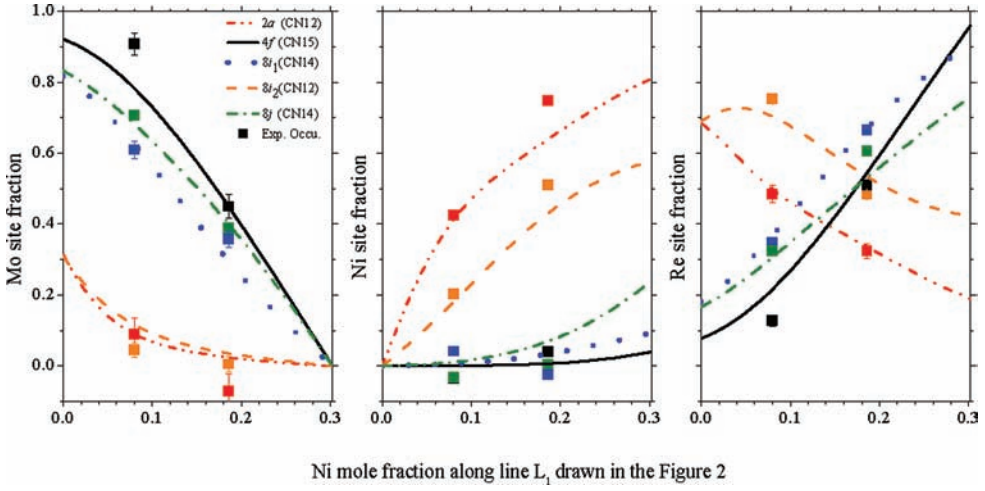

Figure 6. Comparison of the experimental and calculated site occupancies of the Mo−Ni−Re σ phase at 1873 K along the line L_1 of Figure 2. The squares and lines correspond to the experimental (N_1 and N_2) and calculated site occupancies, respectively.

numbers (Z_{Mo} = 42, Z_{Ni} = 28, and Z_{Re} = 75) and Fermi lengths (b_{Mo} = 6.7, b_{Ni} = 10.3, and b_{Re} = 9.2 fm). On the other hand, they also present different scattering contrast in the two considered diffraction techniques; i.e., Ni is the weakest scattering element in the XRD experiment and the strongest in the ND experiment. The fulfillment of both conditions by the studied system made possible the accurate experimental determination of site occupancies.

To study the atomic distribution on different sites as a function of the composition, site occupancies were determined along the two lines named as L_1 and L_2 drawn in Figure 2. The line L_1 has been chosen to pass from the ideal stoichiometry Mo_2Re to $ReNi_2$, whereas line L_2 passes from close to the $MoRe_2$ composition, i.e., $Mo_{0.299}Re_{0.701}$,[21] toward the calculated stable Mo_2Ni composition.

The site occupancies determined along the line L_1 as a function of the Ni content are presented in Figure 6. As shown in the plot, the Mo and Ni site fractions in the Mo−Ni−Re σ phase along the line L_1 show similar variations (either increase or decrease). Ni, whose atomic size is significantly smaller than Mo and Re, substitutes them mainly on the sites with low CN, i.e., 2*a* and 8i_2 (CN = 12). On the other hand, Mo atoms, being the largest in size, tend to occupy high-CN sites, i.e., 4*f*, 8i_1, and 8*j* (CN = 15, 14, and 14), where they can find more space. Contrary to the behavior of Mo and Ni, the Re atoms, being intermediate in size [r_{Ni} (~135 pm) < r_{Re} (~137 pm) < r_{Mo} (~139 pm)], show dual preference depending on the composition proportion of the other two elements. As can be seen from Figure 6, Re prefers occupying the low-CN sites at less Ni content. However, with increasing Ni content along the line L_1, a reversal in the behavior of Re was observed, and it exhibits a preference for occupying the sites with higher CN. This reversal in the preference of Re from the sites of low CN to the sites of high CN is evident not only from the calculated but also from the experimentally determined site occupancies. Therefore, it can be concluded that intermediate-size elements in any ternary σ phase depending on the composition proportion of the other two elements may have a dual preference. The same behavior of intermediate-size elements has also been recently reported in the Cr−Mo−Re σ phase.[3] However, unlike the present study, the dual preference of Re in the Cr−Mo−Re σ phase was evidenced only by DFT calculations, and no experimental investigation was carried out because of the unfavorable scattering factors of the constituent elements.

The plots of the experimental and calculated site occupancies along the line L_2 as a function of the Ni content are presented in Figure 7. The Mo, Ni, and Re site fractions demonstrate either an increase or a decrease with increasing Ni content along the line L_2. The site occupancy results indicated that Mo, being the largest in atomic size, showed a preference for the high-CN sites, whereas Ni and Re atoms, being smaller in atomic size, preferred occupying the sites with low CN. In addition, the calculated site occupancies determined along the

dx.doi.org/10.1021/ic202479y | Inorg. Chem. 2012, 51, 3071−3078

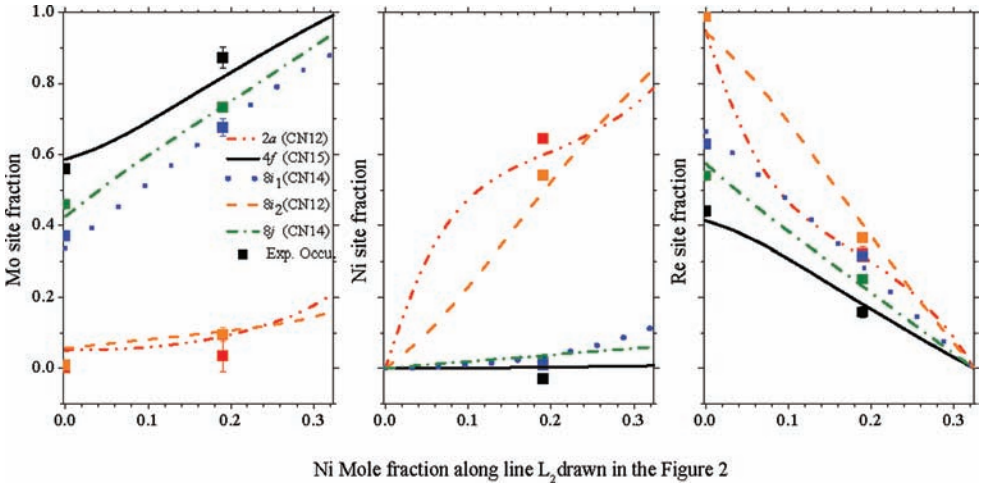

Figure 7. Comparison of the experimental and calculated site occupancies of the Mo−Ni−Re σ phase at 1873 K along the line L_2 of Figure 2. The squares correspond to the experimental (N_3 and experimental data from the literature[21]) site occupancies and the lines to the calculated site occupancies.

line L_2 showed progressive advancement toward Mo_2Ni composition, as expected from the calculated stability of this particular binary composition, which was discussed earlier. This tendency of the σ phase toward ordering is also evident from the experimentally determined site occupancies of σ of composition N_3 and of the σ phase of composition $Mo_{0.701}Re_{0.299}$.

In the Mo−Ni−Re σ phase, contrary to the Cr−Mo−Re σ phase in which the stability domain was parallel to the axis defined by the elements with the largest and smallest atomic radii, the stability line (L_2) is orthogonal to the line in which Re reversal occurs (L_1)

The comparison of the experimental and calculated site occupancies determined during the present investigation is presented in Figures 6 and 7. As can be seen from Figures 6 and 7, an appreciably good agreement was found between the two data, which confirms the validity of both the experimental and calculation techniques. In addition, because calculation of the site occupancies was carried out by using BW approximation, which ignores the short-range-order contributions, therefore, it can be concluded that calculation of the site occupancies even by using BW approximation can produce accurate results for topologically closed-packed phases such as the σ phase. Moreover, the site-occupancy data determined during the present investigation because of its reliability not only can be incorporated as an experimental input for the CALPHAD modeling of the Mo−Ni−Re system but also can be used in the selection of a suitable model for thermodynamic modeling of the σ phase by CALPHAD method. The site occupancies of the ternary σ phase determined during the present investigation, as shown in Figures 6 and 7, can be divided into two groups: one group corresponds to the sites with high CN and the other group corresponds to low-CN sites; which points to the fact that the σ phase can be well described even by using a 2-sublattice model, as was also suggested previously,[1] at least for the present system.

CONCLUSIONS

In the present work, we have shown that it was possible to obtain accurate site occupancies for complex ternary intermetallic compounds not only experimentally by using the combined refinement of XRD and ND data but also by calculating, in the frame of the DFT, the complete set of ordered configurations of the phase in the complete ternary range of composition. The agreement between these two kinds of determination has been found to be excellent. This may be considered as a confirmation of the validity of both techniques. Though difficult, making such a determination is particularly worthwhile for ternary systems in which the same element may play different roles regarding the two other elements and therefore show a reversal of its properties along the ternary existence range of the phase. Making more systematic studies on this subject is still an open field for future research.

ASSOCIATED CONTENT

Supporting Information

CIFs of the experimentally studied compositions and an additional table containing the complete list of calculated formation enthalpies and the crystallographic parameters of every relaxed Mo−Ni−Re-ordered configuration in the σ-phase structure. This material is available free of charge via the Internet at http://pubs.acs.org.

AUTHOR INFORMATION

Corresponding Author

*E-mail: jean-marc.joubert@icmpe.cnrs.fr.

Notes

The authors declare no competing financial interest.

ACKNOWLEDGMENTS

Financial support from the Agence Nationale de la Recherche (Project Armide 2010 BLAN 912 01) is acknowledged. The authors thank Florence Porcher of LLB, Saclay, France, for carrying out ND experiments and Eric Leroy for EPMA measurements. DFT calculations were performed using HPC resources from GENCI-CINES (Grant 2011-96175).

REFERENCES

(1) Joubert, J.-M. *Prog. Mater. Sci.* **2008**, *53*, 528−583.
(2) Tobola, J.; François, M.; Elkaim, E.; Joubert, J.-M.; Vilasi, M. *Intermetallics* **2010**, *18*, 781−790.
(3) Crivello, J.-C.; Palumbo, M.; Abe, T.; Joubert, J.-M. *CALPHAD: Comput. Coupling Phase Diagrams Thermochem.* **2010**, *34*, 487−494.
(4) Palumbo, M.; Taichi, A.; Fries, S. G.; Pasturel, A. *Phys. Rev.* **2011**, *B83*, 144109.

(5) Yaqoob, K.; Joubert, J.-M. To be published.
(6) Fries, S. G.; Sundman, B. *Phys. Rev.* **2002**, *B66*, 012203.
(7) Korzhavyi, P. A.; Sundman, B.; Selleby, M.; Johansson, B. *Mater. Res. Soc. Symp. Proc.* **2005**, *842*, S4.10.11−16.
(8) Crivello, J.-C.; Joubert, J.-M. *J. Phys.: Condens. Matter* **2010**, *22*, 035402.
(9) Rodríguez-Carvajal, J. XV Congress of International Union of Crystallography, Satellite Meeting on Powder Diffraction, 1990; p 127.
(10) Kresse, G.; Furthmüller, J. *Phys. Rev. B* **1996**, *54*, 11169−11186.
(11) Kresse, G.; Joubert, D. *Phys. Rev. B* **1999**, *59*, 1758.
(12) Palumbo, M.; Abe, T.; Kocer, C.; Murakami, H.; Onodera, H. *CALPHAD: Comput. Coupling Phase Diagrams Thermochem.* **2010**, *34*, 495−503.
(13) Perdew, J. P.; Wang, Y. *Phys. Rev. B* **1992**, *45*, 13244−13249.
(14) Perdew, J. P.; Burke, K.; Ernzerhof, M. *Phys. Rev. Lett.* **1997**, *78*, 1396.
(15) Monkhorst, H. J.; Pack, J. D. *Phys. Rev.* **1976**, *B13*, 5188−5192.
(16) Blöchl, P. E.; Jepsen, O.; Andersen, O. K. *Phys. Rev.* **1994**, *B49*, 16223.
(17) Sundman, B.; Ågren, J. *J. Phys. Chem. Solids* **1981**, *42*, 297−301.
(18) Ansara, I.; Dupin, N.; Sundman, B. *CALPHAD* **1997**, *21*, 535−542.
(19) Ansara, I.; Burton, B.; Chen, Q.; Hillert, M.; Fernandez Guillermet, A.; Fries, S. G.; Lukas, H. L.; Seifert, H. J.; Oates, W. A. *CALPHAD* **2000**, *24*, 19−40.
(20) Brewer, L.; Lamoreaux, R. H. *At. Energy Rev.* **1980**, No. Spec. Issue 7, 195−356.
(21) Farzadfar, S.-A.; Levesque, M.; Phejar, M.; Joubert, J.-M. *CALPHAD: Comput. Coupling Phase Diagrams Thermochem.* **2009**, *33*, 502−510.
(22) Joubert, J.-M.; Cerný, R.; Latroche, M.; Percheron-Guégan, A.; Yvon, K. *J. Appl. Crystallogr.* **1998**, *31*, 327−332.
(23) Joubert, J.-M. *CALPHAD* **2002**, *26*, 419−425.
(24) Joubert, J.-M. *CALPHAD* **2002**, *26*, 427−438.
(25) Seiser, B.; Drautz, R.; Pettifor, D. G. *Acta Mater.* **2011**, *59*, 749−763.